

Iron–Gold (or –Mercury) Carbide Clusters Derived from $[\text{Fe}_6\text{C}(\text{CO})_{16}]^{2-}$. X-ray Crystal Structures of $(\text{NEt}_4)[\text{Fe}_6\text{C}\{\text{AuPPh}_3\}(\text{CO})_{16}]$ and $[\text{Fe}_4\text{C}\{\text{AuPPh}_3\}(\text{CO})_{11}(\text{NO})]$

Oriol Rossell,* Miquel Seco,* Glòria Segalés, and Santiago Alvarez

Departament de Química Inorgànica, Universitat de Barcelona, Diagonal 647, E-08028 Barcelona, Spain

Maria Angela Pellinghelli and Antonio Tiripicchio*

Dipartimento di Chimica Generale ed Inorganica, Chimica Analitica, Chimica Fisica, Università di Parma, Centro di Studio per la Strutturistica Diffattometrica del CNR, Viale delle Scienze 78, I-43100 Parma, Italy

Dominique de Montauzon

Laboratoire de Chimie de Coordination du CNRS, 205 route de Narbonne, F-31077 Toulouse Cedex, France

Received July 15, 1996[⊗]

The metal halide complexes ClAuPPh_3 and $\text{ClHg}(\text{m})$ react in thf with $[\text{Fe}_6\text{C}(\text{CO})_{16}]^{2-}$ affording the metal cluster compounds $(\text{NEt}_4)[\text{Fe}_6\text{C}\{\mu_3\text{-AuPPh}_3\}(\text{CO})_{16}]$ (**1**) and $(\text{NEt}_4)[\text{Fe}_6\text{C}\{\text{Hg}(\text{m})\}(\text{CO})_{16}]$ ($\text{m} = \text{Mo}(\text{CO})_3\text{Cp}$ (**2**), $\text{W}(\text{CO})_3\text{Cp}$ (**3**), and $\text{Mn}(\text{CO})_5$ (**4**)) in good yields. The cluster $[\{\text{Fe}_6\text{C}(\text{CO})_{16}\}_2(\text{Hg})]^{2-}$ (**5**) is also isolated by reaction of this anion with $\text{Hg}(\text{NO}_3)_2$. The product obtained by treatment of **1** with NOBF_4 depends on the stoichiometry of the reaction. Thus, with a 1:1 molar ratio the nitrosyl compound $[\text{Fe}_6\text{C}\{\text{AuPPh}_3\}(\text{CO})_{15}(\text{NO})]$ (**6**) was formed whereas the use of an excess of NOBF_4 led to the pentametal cluster $[\text{Fe}_4\text{C}\{\text{AuPPh}_3\}(\text{CO})_{11}(\text{NO})]$ (**7**). The structures of **1** and **7** have been determined by X-ray diffraction methods. The electrochemical behavior of **2–5** has been investigated by cyclic voltammetry and coulometry. An extended Hückel molecular orbital study of the bonding capabilities of $[\text{Fe}_4\text{C}(\text{CO})_{12}]^{2-}$ has been carried out in order to understand the structural differences between $[\text{Fe}_4\text{C}\{\text{AuPPh}_3\}(\text{CO})_{12}]^-$ and $[\text{HFe}_4\text{C}(\text{CO})_{12}]^-$.

Introduction

Iron carbonyl anions have been widely used for the synthesis of mixed-metal clusters, especially those containing group 11 and 12 elements. Thus, for instance, linear Fe_2M ($\text{M} = \text{Zn}, \text{Cd}, \text{Hg}$), triangular Fe_2M ($\text{M} = \text{Au}, \text{Hg}, \text{Cu}^+$) and FeAu_2 ,⁵ square-planar Fe_2Au_2 ,⁶ butterfly Fe_3M ($\text{M} = \text{Au}, \text{Hg}$)⁷ and Fe_2Cu_2 ,⁸ square-pyramid Fe_3Au_2 ,⁹ and bow-tie Fe_4Au ¹⁰ metal clusters have been reported to date. Moreover, heteronuclear metal clusters exhibiting more complicated

structures have also been obtained by using iron carbide,¹¹ nitride,¹² or boride¹³ anions as reagents. It is worth noting that the geometry of the clusters obtained from the reaction between $[\text{Fe}_4(\text{CO})_{13}]^{2-}$ and metal halide complexes, such as ClMPr_3 ($\text{M} = \text{Cu}, \text{Au}$) or ClHgCH_3 , exceptionally depends on the nature of the metal fragment.¹⁴ For example, while $[\text{Fe}_4(\text{CuPPh}_3)(\text{CO})_{13}]^-$ displays a tetrahedral iron core, the iron skeleton of the corresponding gold derivative, $[\text{Fe}_4(\text{AuPEt}_3)(\text{CO})_{13}]^-$, opens into a butterfly geometry which forces one CO ligand to take up an unusual bridging coordination mode to conform the polyhedral skeletal electron-pair theory. Remarkably, the $[\text{Fe}_4(\text{HgCH}_3)(\text{CO})_{13}]^-$ anion can be crystallized in both forms, depending on the solvent. From all of these results, it seemed interesting to extend our studies to other iron carbonyl anions showing higher nuclearities in order to compare their reactivity with the metal fragments AuPPh_3^+ and $\text{Hg}(\text{m})^+$ ($\text{m} = \text{Mo}(\text{CO})_3\text{Cp}$,

[⊗] Abstract published in *Advance ACS Abstracts*, December 1, 1996.

(1) (a) Sosinsky, B. A.; Shong, R. G.; Fitzgerald, B. J.; Norem, N.; O'Rourke, C. *Inorg. Chem.* **1983**, *22*, 3124. (b) Alvarez, S.; Ferrer, M.; Reina, R.; Rossell, O.; Seco, M.; Solans, X. *J. Organomet. Chem.* **1989**, *377*, 291.

(2) Rossell, O.; Seco, M.; Jones, P. G. *Inorg. Chem.* **1990**, *29*, 348. (3) Reina, R.; Rossell, O.; Seco, M. *J. Organomet. Chem.* **1990**, *398*, 285.

(4) Ferrer, M.; Reina, R.; Rossell, O.; Seco, M.; Solans, X. *J. Chem. Soc., Dalton Trans.* **1991**, 347.

(5) Albano, V. G.; Calderoni, F.; Iapalucci, M. C.; Longoni, G.; Monari, M. *J. Chem. Soc., Chem. Commun.* **1995**, 433.

(6) Alvarez, S.; Rossell, O.; Seco, M.; Valls, J.; Pellinghelli, M. A.; Tiripicchio, A. *Organometallics* **1991**, *10*, 2309.

(7) (a) Rossell, O.; Seco, M.; Reina, R.; Font-Bardía, M.; Solans, X. *Organometallics* **1994**, *13*, 2127. (b) Reina, R.; Rossell, O.; Seco, M.; de Montauzon, D.; Zquiak, R. *Organometallics* **1994**, *13*, 4300.

(8) Deng, H. G.; Shore, S. G. *Organometallics* **1991**, *10*, 3486.

(9) Roland, E.; Fischer, K.; Vahrenkamp, H. *Angew. Chem., Int. Ed. Engl.* **1983**, *22*, 326.

(10) Albano, V. G.; Aureli, R.; Iapalucci, M. C.; Laschi, F.; Longoni, G.; Monari, M.; Zanello, P. *J. Chem. Soc., Chem. Commun.* **1993**, 1501.

(11) (a) Johnson, B. F. G.; Kaner, D. A.; Lewis, J.; Raitby, P. R.; Rosales, M. J. *J. Organomet. Chem.* **1982**, *231*, C59. (b) Johnson, B. F. G.; Kaner, D. A.; Lewis, J.; Rosales, M. J. *J. Organomet. Chem.* **1982**, *238*, C73.

(12) Blohm, M. L.; Gladfelter, W. L. *Inorg. Chem.* **1987**, *26*, 459. (13) Housecroft, C. E.; Shongwe, M. S.; Rheingold, A. L. *Organometallics* **1989**, *8*, 2651.

(14) Horwitz, C. P.; Holt, E. M.; Brock, C. P.; Shriver, D. F. *J. Am. Chem. Soc.* **1985**, *107*, 8136.

W(CO)₃Cp, Mn(CO)₅) and to determine the geometry of the resulting metal cluster compounds. Specifically, we were interested in obtaining the first compound in which an iron triangular face is capped by an AuPR₃ fragment in order to compare the resulting gold–iron distances with those reported for metal systems involving gold fragments bonded to only one iron atom¹⁵ or bridging Fe–Fe edges.^{6,11b,14,16} As a starting anion, we chose the carbido cluster [Fe₆C(CO)₁₆]²⁻ which was assumed to be a good nucleophile agent because of its two-negative charge. Additionally, the presence of the four-electron carbido ligand would favor the stabilization of the final products, as has been shown for similar ruthenium clusters.¹⁷ We report here the synthesis of the heptanuclear [Fe₆C{AuPPh₃}₃(CO)₁₆]⁻ and the octanuclear species [Fe₆C{Hg(m)}₂(CO)₁₆]⁻ (m = Mo(CO)₃Cp, W(CO)₃Cp, Mn(CO)₅), obtained by reacting the starting carbido cluster [Fe₆C(CO)₁₆]²⁻ with gold and mercury halide derivatives, respectively. The electrochemical behavior of the mercury compounds has been investigated and the X-ray crystal structure of the gold derivative has been determined. The reactivity of [Fe₆C{AuPPh₃}₃(CO)₁₆]⁻ with NOBF₄ was examined in an attempt to obtain the neutral compound [Fe₆C{AuPPh₃}₃(CO)₁₅(NO)], but the resulting complex was found to be [Fe₄C{AuPPh₃}₃(CO)₁₁(NO)] by an X-ray diffraction investigation.

Results and Discussion

Treatment of [NEt₄]₂[Fe₆C(CO)₁₆] with ClAuPPh₃ (1:1 molar ratio) in tetrahydrofuran (thf) at -15 °C in the presence of TIBF₄ as a halide abstractor afforded the new black crystalline compound [NEt₄][Fe₆C{AuPPh₃}₃(CO)₁₆] (**1**) in good yield. By a similar procedure, employing the halide complexes ClHg(m) (m = Mo(CO)₃Cp, W(CO)₃Cp, Mn(CO)₅), the clusters [NEt₄][Fe₆C{HgMo(CO)₃Cp}₂(CO)₁₆] (**2**), [NEt₄][Fe₆C{HgW(CO)₃Cp}₂(CO)₁₆] (**3**), and [NEt₄][Fe₆C{HgMn(CO)₅}₂(CO)₁₆] (**4**) were isolated. However, in these cases an excess of ClHg(m) was required to complete the reaction. The ν(CO) IR pattern of **1** was almost superimposable on those observed for **2–4** if the bands due to the m part are ignored. This is not surprising taking into account the isolobal relationship¹⁸ between AuPR₃⁺ and Hg(m)⁺. In particular, the highest-wavenumber band is shifted to frequencies 20–30 cm⁻¹ higher than that of the starting iron anion¹⁹ indicating a decrease in electron density in the iron atoms. The band at ca. 1800–1820 cm⁻¹ indicates the presence of bridging carbonyl ligands in each case. When **1** was treated under FABS conditions, the peak due to the parent ion was much lower than that attributable to the other species generated.

(15) (a) Arndt, L. W.; Darensbourg, M. Y.; Fackler, J. P., Jr.; Lusk, R. J.; Marler, D. O.; Youngdahl, K. A. *J. Am. Chem. Soc.* **1985**, *107*, 7218. (b) Simon, F. E.; Lahuer, J. W. *Inorg. Chem.* **1980**, *19*, 2338. (c) Schlubert, U.; Kunz, E.; Knorr, M.; Muller, J. *Chem. Ber.* **1987**, *120*, 1079.

(16) (a) Horwitz, C. P.; Holt, E. M.; Shriver, D. F. *J. Am. Chem. Soc.* **1985**, *107*, 281. (b) Bruce, M. I.; Nicholson, B. K. *J. Organomet. Chem.* **1983**, *250*, 627. (c) Umland, H.; Behrens, U. *J. Organomet. Chem.* **1985**, *287*, 109. (d) Aitchison, A. A.; Farrugia, L. J. *Organometallics* **1986**, *5*, 1103.

(17) Bailey, P. J.; Beswick, M. A.; Lewis, J.; Raithby, P. R.; Ramirez de Arellano, M. C. *J. Organomet. Chem.* **1993**, *459*, 293.

(18) Lahuer, J. W.; Wald, K. *J. Am. Chem. Soc.* **1981**, *103*, 7648.

(19) (a) Churchill, M. R.; Wormald, J. *J. Chem. Soc., Dalton Trans.* **1974**, 2410. (b) Hill, E. W.; Bradley, J. S. *Inorg. Synth.* **1987**, *27*, 182.

However, the electrospray mass spectra (ESMS) for **1** were more informative and, thus, the spectrum at a skimming voltage of 50 V showed only two peaks, the most intense attributable to the parent ion and the second to the species corresponding to the loss of one carbonyl ligand. In contrast, for compounds **2–4** the most intense peaks of the ESMS spectra, under the same conditions, corresponded to the loss of four and five carbonyl ligands and a small parent ion peak was observed only for **2**. That the carbonyl groups in **1** are more strongly attached to the iron atoms than they are in **2–4** (in the ESMS experiments) is in agreement with the shift to higher frequencies of the ν(CO) bands in going from **1** to **2–4**.

Neither **1** nor the complexes **2–4** reacted with an excess of the gold or the mercury complexes to give clusters with higher nuclearities, this behavior being in good accord with that observed in other metal systems.^{2,6} Moreover, these iron clusters tend to lose the coordinated gold or mercury fragment. This is easily shown for [NEt₄][Fe₆C{AuPPh₃}₃(CO)₁₆], which at temperature above 60 °C ejects the AuPPh₃ moiety. In addition, the mercury-containing clusters **2–4** undergo partial metal–ligand redistribution reactions in solution. This type of process is well-known, and the factors favoring the stability of the symmetric compound over the asymmetric one have recently been discussed.^{3,7} In general, the presence of some negative charge on the asymmetric species stabilizes it against the symmetrization by precluding the associative process proposed for this type of reaction.²⁰ Because of the large delocalization of the negative charge over the eight metal atoms, complexes **2–4** show a slight tendency to the symmetrization, indicated by the presence of small quantities of m₂Hg compounds as well as an unchanging weak signal at 2010 cm⁻¹, which could correspond to the dianion [Fe₆C(CO)₁₆]₂(Hg)²⁻ (**5**). This hypothesis was confirmed later when the latter cluster from the reaction between [NEt₄]₂[Fe₆C(CO)₁₆] and Hg(NO₃)₂ was isolated at room temperature in thf solution.

No species resulting from the partial degradation of the Fe₆C skeleton was detected during the formation of **1–4**, probably as a consequence of the presence of the carbido carbon atom, which stabilizes the metal core. The analogous ruthenium/gold cluster, [Ru₆C{AuPMePh₂}₂(CO)₁₆], obtained by the same procedure, was also shown to be stable.²¹ However, the similarity between the iron and the ruthenium compounds is broken when the reaction of the anions [M₆C(CO)₁₆]²⁻ (M = Fe, Ru) with (ClAu)₂(μ-dppm) is compared. Thus, for M = Ru,¹⁷ the final product was [Ru₆CAu₂(CO)₁₆(μ-dppm)] while, for M = Fe, the cluster [Fe₄CAu₂(CO)₁₂(μ-dppm)]²² was isolated. This example shows the difference in thermodynamic stability between the iron and ruthenium clusters as correspond to metal atoms belonging to the first and second periods, respectively.

We were also interested in obtaining nitrosyl-containing metal clusters because the coordinated NO ligand

(20) Abraham, M. H. *Comprehensive Chemical Kinetics*; Bamford, C. H., Tipper, C. F. H., Eds.; Elsevier: Amsterdam, 1973; Vol. 12.

(21) Bunkhall, J. R.; Holden, H. D.; Johnson, B. F. G.; Lewis, J.; Pain, G. N.; Raithby, P. R.; Taylor, M. J. *J. Chem. Soc., Chem. Commun.* **1984**, 25.

(22) Rossell, O.; Seco, M.; Segalés, G.; Johnson, B. F. G.; Dyson, P. J.; Ingham, S. L. *Organometallics* **1996**, *15*, 884.

is susceptible to hydrogenation,²³ electrophilic attack,²⁴ and deoxygenation²⁵ to yield nitrido clusters. For this purpose, two ways were considered: (i) the use of the nitrosyl-containing anion²⁶ $[\text{Fe}_6\text{C}(\text{CO})_{15}(\text{NO})]^-$; (ii) the reaction of the gold cluster **1** with NOBF_4 . The first was unsuccessful because of the poor nucleophilicity of the anion, which precluded the reaction with ClAuPPh_3 even in the presence of TIBF_4 as a halide abstractor. The second gave more interesting results, which depended on the molar ratio of the reagents. If **1** was reacted in thf with NOBF_4 , the main product was the neutral compound $[\text{Fe}_6\text{C}\{\text{AuPPh}_3\}(\text{CO})_{15}(\text{NO})]$ (**6**), according to its IR ($\nu(\text{NO}) = 1754 \text{ cm}^{-1}$) and ^{31}P NMR spectra ($\delta(^{31}\text{P}) = 54.0 \text{ ppm}$); however, the addition of an excess of the nitrosyl compound (1:4 molar ratio) to the solution afforded dark green crystals of a compound which was formulated as $[\text{Fe}_4\text{C}\{\text{AuPPh}_3\}(\text{CO})_{11}(\text{NO})]$ (**7**). It is interesting to note that in (ii) traces of **7** always appear together with **6**, and it was shown experimentally that **7** results from the partial degradation of **6**. This is not very surprising given the ability of the NO^+ species to oxidize the metal clusters.²⁷ The nature of **7** has been elucidated on the basis of an X-ray study and IR and NMR spectroscopies. Despite the fact that the NO ligand could not be unambiguously located, some structural evidence about its location was obtained (see below). Moreover, besides the elemental analysis, the following features indirectly confirm its presence: (i) No hydride signal was detected at high fields in the ^1H NMR spectrum, which rules out the compound $[\text{HFe}_4\text{C}\{\text{AuPPh}_3\}(\text{CO})_{12}]$. (ii) The ^{13}C NMR spectrum showed three types of carbon atom in the carbonyl region, with a relative intensity 2:3:6, in contrast with the two different carbon atoms (6:6) shown in the spectrum of $[\text{Fe}_4\text{C}(\text{CO})_{12}]^{2-}$. (iii) A band of medium intensity at 1762 cm^{-1} in the IR spectrum was unequivocally assigned to the NO group, given that no bridging carbonyl ligands are present in the X-ray crystal structure of **7**. (iv) A peak was found in the FABS(-) spectrum of **7**, corresponding to the $\text{M} - 2\text{CO}$ fragment.

Finally, it should be noted that the ruthenium analog of **6**, that is $[\text{Ru}_6\text{C}\{\text{AuPPh}_3\}(\text{CO})_{15}(\text{NO})]$, has been synthesized by procedure (i) due to the greater nucleophilicity of the ruthenium anion.²⁸ In contrast, the corresponding ruthenium compound of **7** has not been reported.

Description of the Crystal Structure of $(\text{NET}_4)\text{-}[\text{Fe}_6\text{C}\{\text{AuPPh}_3\}(\text{CO})_{16}]$ (1**).** In the crystals of **1**, $[\text{Fe}_6\text{C}\{\text{AuPPh}_3\}(\text{CO})_{16}]^-$ anions and $[\text{NET}_4]^+$ cations are present. The structure of the anion is shown in Figure 1, together with the atomic numbering scheme; the most significant bond distances and angles are given in Table 1. The structure may be regarded as derived from that of $[\text{Fe}_6\text{C}(\text{CO})_{16}]^{2-}$ by capping one triangular face of the slightly distorted octahedron by the AuPPh_3^+ frag-

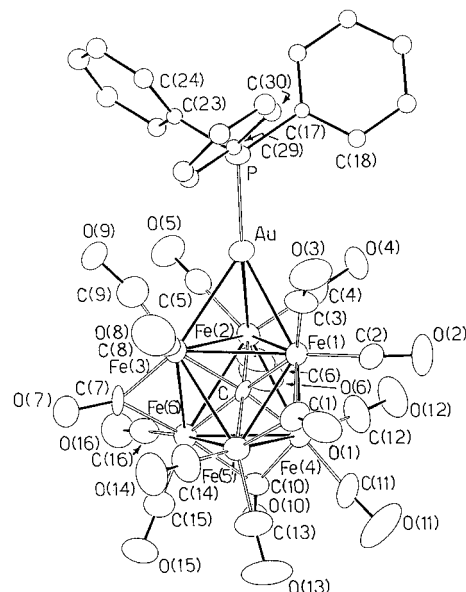


Figure 1. ORTEP view of the molecular structure of the anion $[\text{Fe}_6\text{C}\{\text{AuPPh}_3\}(\text{CO})_{16}]^-$ (**1**) together with the atomic numbering scheme. The ellipsoids for the atoms are drawn at the 30% probability level.

Table 1. Selected Bond Distances (Å) and Angles (deg) for **1**

Au-Fe(1)	2.733(2)	Au-Fe(3)	2.732(3)
Au-Fe(2)	2.785(2)	Au-P	2.295(4)
Fe(1)-Fe(2)	2.801(4)	Fe(1)-Fe(3)	2.767(4)
Fe(1)-Fe(4)	2.715(4)	Fe(1)-Fe(5)	2.562(3)
Fe(2)-Fe(3)	2.716(3)	Fe(2)-Fe(4)	2.646(4)
Fe(2)-Fe(6)	2.747(3)	Fe(3)-Fe(5)	2.710(3)
Fe(3)-Fe(6)	2.601(3)	Fe(4)-Fe(5)	2.694(4)
Fe(4)-Fe(6)	2.618(4)	Fe(5)-Fe(6)	2.664(4)
Fe-C mean	1.901(15)		
Fe(1)-C-Fe(6)	172.1(9)	Fe(1)-C(1)-Fe(5)	82.0(8)
Fe(3)-C-Fe(4)	172.6(9)	Fe(3)-C(7)-Fe(6)	82.8(7)
Fe(2)-C-Fe(5)	179.0(8)	Fe(4)-C(10)-Fe(6)	79.6(7)

ment.¹⁹ Interestingly, this is the first example reported in which a gold atom is bonded simultaneously to three iron atoms in a μ_3 bonding mode. Here, the AuPPh_3^+ unit caps one of the two triangular faces of the $[\text{Fe}_6\text{C}(\text{CO})_{16}]^{2-}$ anion lacking bridging carbonyl ligands; as a consequence, the resulting cluster has lost the mirror plane present in the dianion. Of the five carbonyl ligands surrounding the gold atom area three belonging to three different iron atoms are bent toward this metal [$\text{Fe}(1)-\text{C}(3)-\text{O}(3) = 169.4(19)$, $\text{Fe}(2)-\text{C}(4)-\text{O}(4) = 167.1(18)$, and $\text{Fe}(3)-\text{C}(9)-\text{O}(9) = 169.7(20)^\circ$]. This behavior has been reported in other Au and Hg complexes and has been described as the result of a partial electron density donation from the $\text{M}-\text{Au}$ (or $-\text{Hg}$) σ bond toward $\pi^*(\text{CO})$ orbitals.^{1b}

Considering that the AuPPh_3^+ fragment contributes with 12 electrons to the polyhedral electron count of the cluster, **1** conforms to the number of electrons (98) expected for this geometry according to the condensation rules given by the polyhedral skeletal electron pair theory. There are 13 terminal carbonyls and three are bridging [$\text{C}(1)-\text{O}(1)$, $\text{C}(7)-\text{O}(7)$, and $\text{C}(10)-\text{O}(10)$]. Fe(2) is the only iron atom that does not participate in a bridging carbonyl system. As expected, the metal-metal distances of the bridged iron-iron bonds appear notably shorter than the unbridged ones. The gold coordination to the $\text{Fe}(1)\text{Fe}(2)\text{Fe}(3)$ face causes an

(23) (a) Johnson, B. F. G.; Lewis, J.; Mace, J. M. *J. Chem. Soc., Chem. Commun.* **1984**, 186. (b) Smieja, J. A.; Stevens, R. E.; Fjare, D. E.; Gladfelter, W. L. *Inorg. Chem.* **1985**, *24*, 3206.

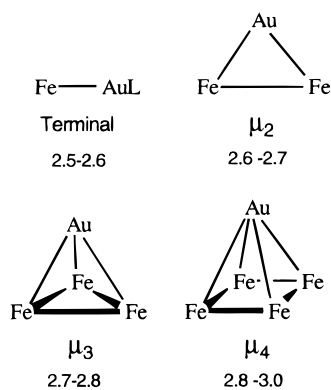
(24) Stevens, R. E.; Gladfelter, W. L. *J. Am. Chem. Soc.* **1982**, *104*, 6454.

(25) Fjare, D. E.; Gladfelter, W. L. *J. Am. Chem. Soc.* **1984**, *106*, 4799.

(26) Gourdon, A.; Jeannin, Y. *J. Organomet. Chem.* **1985**, *282*, C39.

(27) Fjare, D. E.; Keynes, D. G.; Gladfelter, W. L. *J. Organomet. Chem.* **1983**, *250*, 383.

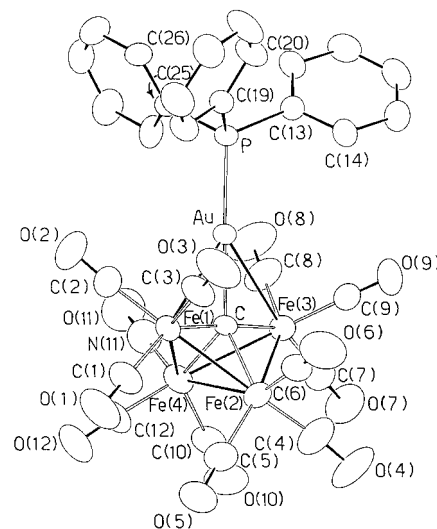
(28) Johnson, B. F. G.; Lewis, J.; Nelson, W. J. H.; Puga, J.; Raithby, P. R.; Braga, D.; McPartlin, M.; Clegg, W. *J. Organomet. Chem.* **1983**, *243*, C13.

Chart 1. Variation of the Fe–Au Bond Lengths (Å) According to the Bonding Mode

appreciable lengthening in the distances between these iron metals, in comparison with the corresponding iron–iron bonds in $[\text{Fe}_6\text{C}(\text{CO})_{16}]^{2-}$. The carbide is roughly equidistant from the six iron atoms with Fe–C distances [in the range 1.853(15)–1.931(14) Å] not significantly different from those reported for the parent anion,¹⁹ even if it can be envisaged as slightly pushed toward the Fe(1)Fe(2)Fe(4) face.

Since **1** represents the first example of an Fe–Au cluster in which the gold atom is bonded in a μ_3 -mode, it seemed interesting to compare its Au–Fe bond distances with those reported for other Fe–Au systems. Here, the three values of the Fe–Au bonds, 2.733(3), 2.785(2), and 2.732(3) Å, are somewhat longer than those reported for the Fe_2 – AuPR_3 (μ_2 -mode) (2.60–2.70 Å)¹⁶ and much longer than those reported for terminal Au–Fe bonds (2.50–2.60 Å).¹⁵ Interestingly, a compound displaying a μ_4 -AuPR bonding mode, $[\text{Fe}_5\text{C}\{\text{AuPEt}_3\}_2(\text{CO})_{14}]$, has been reported^{11b} and the values of the Fe–Au distances (2.83–3.04 Å) are also somewhat longer than those found in **1**. In conclusion, an increase in the coordination number of the gold atom promotes a gradual lengthening of the gold–iron distances (Chart 1).

Description of the Crystal Structure of $[\text{Fe}_4\text{C}\{\text{AuPPh}_3\}(\text{CO})_{11}(\text{NO})]$ (7**).** The molecular structure of **7** is shown in Figure 2 together with the atomic numbering scheme. Selected bond distances and angles are given in Table 2. The four iron atoms are in a butterfly arrangement while the Au atom bridges the two wingtip iron atoms. The dihedral angle between the Fe(1)Fe(2)Fe(4) and Fe(2)Fe(4)Fe(3) planes is 107.3(1)°. The carbido atom occupies the cavity of the Fe_4Au metal core and is bonded to all five metal atoms almost collinear to the wingtip atoms [the Fe(1)–C–Fe(3) angle is 176.1(5)°]. The C(carbido)–Fe(wingtip) distances, 1.861(7) and 1.845(7) Å, are slightly shorter than those with the hinge Fe atoms, 1.915(9) and 1.926(8) Å, whereas the Fe–Fe bond lengths, in the range 2.578(2)–2.657(2) Å, fall in the expected range. The whole Fe_4C fragment is very similar to that found in other known butterflies of this type (see below). The Fe–Au bond distances, 2.820(2) and 2.866(2) Å, are very similar to those found in the related compounds $[\text{Fe}_4\text{C}\{\text{AuPPh}_3\}(\mu\text{-H})(\text{CO})_{12}]^{11a}$ and $[\text{Fe}_4\text{CAu}_2(\text{CO})_{12}(\mu\text{-dppm})]^{22}$. The value of the Au–C distance, 2.095(9) Å, is also comparable to those found in these complexes and in other compounds with Au–C single bonds.²⁹

**Figure 2.** ORTEP view of the molecular structure of $[\text{Fe}_4\text{C}\{\text{AuPPh}_3\}(\text{CO})_{11}(\text{NO})]$ (**7**) together with the atomic numbering scheme. The ellipsoids for the atoms are drawn at the 30% probability level.**Table 2. Selected Bond Distances (Å) and Angles (deg) for **7****

Fe(1)–Fe(2)	2.625(2)	Au–C	2.095(9)
Fe(1)–Fe(4)	2.635(2)	Fe(1)–C	1.861(7)
Fe(2)–Fe(3)	2.626(2)	Fe(2)–C	1.915(9)
Fe(3)–Fe(4)	2.657(2)	Fe(3)–C	1.845(7)
Fe(2)–Fe(4)	2.578(2)	Fe(4)–C	1.926(8)
Au–Fe(1)	2.820(2)	Au–P	2.273(3)
Au–Fe(3)	2.866(2)		
Fe(1)–Au–Fe(3)	81.3(1)	Fe(1)–C–Fe(2)	88.1(3)
Fe(2)–Fe(1)–Fe(4)	58.7(1)	Fe(1)–C–Fe(3)	176.1(5)
Fe(1)–Fe(2)–Fe(4)	60.9(1)	Fe(1)–C–Fe(4)	88.2(3)
Fe(1)–Fe(2)–Fe(3)	89.7(1)	Fe(1)–C–Au	90.7(4)
Fe(3)–Fe(2)–Fe(4)	61.4(1)	Fe(2)–C–Fe(3)	88.6(4)
Fe(2)–Fe(3)–Fe(4)	58.4(1)	Fe(2)–C–Fe(4)	84.3(3)
Fe(2)–Fe(4)–Fe(3)	60.2(1)	Fe(2)–C–Au	146.3(5)
Fe(1)–Fe(4)–Fe(3)	88.8(1)	Fe(3)–C–Fe(4)	89.6(4)
Fe(1)–Fe(4)–Fe(2)	60.4(1)	Fe(3)–C–Au	93.1(3)
P–Au–C	176.5(2)	Fe(4)–C–Au	129.3(4)

All 11 carbonyls and the nitrosyl are terminal. Even if it is very difficult to distinguish the nitrosyl group from the carbonyls, in this case there is evidence about its location (see Experimental Section). The Fe(4)–N(11) bond distance involving the nitrosyl ligand, 1.729(11) Å, is, as expected, shorter than the Fe–C ones involving carbonyls, which are in the range 1.756(14)–1.815(2) Å, in agreement with the mean values of these distances, 1.67 and 1.78 Å, respectively, reported in the Cambridge Structural Database (CSD).

Electrochemistry of Compounds $(\text{Et}_4\text{N})[\text{Fe}_6\text{C}\{\text{Hg}(\text{m})\}(\text{CO})_{16}]$ (2–4**) and $(\text{Et}_4\text{N})_2[\text{Fe}_6\text{C}(\text{CO})_{16}]^{2-}$ (**Hg**) (**5**).** The electrochemical properties of the title compounds were studied in CH_2Cl_2 to compare their electrochemical behavior with that of related systems. Figure 3 shows the cyclic voltammogram of the anion **3** in CH_2Cl_2 – Bu_4NPF_6 (0.1 M) solution at 0.1 V s^{-1} . An irreversible oxidation wave at 0.87 V (I) and an irreversible reduction wave at –0.77 V (II) were observed with the same magnitude. The same pattern was observed for all studied compounds (Table 5); other

(29) (a) Fernández, E. J.; Gimeno, M. C.; Jones, P. G.; Laguna, A.; Laguna, M.; Lopez-de-Luzuriaga, J. M. *Angew. Chem., Int. Ed. Engl.* **1994**, *33*, 87. (b) Laguna, A.; Laguna, M.; Jiménez, J.; Lahoz, F. J.; Olmos, E. *Organometallics* **1994**, *13*, 253.

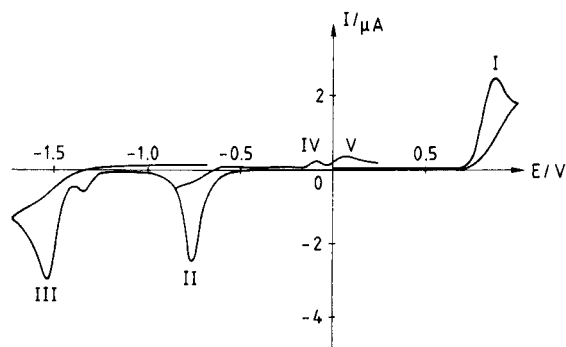
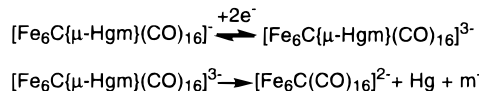


Figure 3. Cyclic voltammogram of compound **3** at 0.1 V/s in $\text{CH}_2\text{Cl}_2\text{-Bu}_4\text{NPF}_6$ (0.1 M).

Scheme 1



peaks were also observed at 1.0 and 1.3 V in the anodic direction and at -1.35 V in the cathodic region which cannot be attributed. In all cases an irreversible wave appeared at -1.53 V (III), which was characterized as the reduction step of $[\text{Fe}_6\text{C}(\text{CO})_{16}]^{2\ominus}$.³⁰ Indeed controlled-potential coulometry at -1.2 V for compounds **3** and **4** required 2 Faradays/mol and resulted in the formation of peaks III and IV, which can be attributed to $[\text{Fe}_6\text{C}(\text{CO})_{16}]^{2\ominus}$ and m^- species, respectively;^{30,7,31} these species can be also detected by IR spectroscopy. Peak V probably corresponds to the reoxidation of free mercury generated by cleavage of the compound. Moreover, the electrochemical oxidation of this reduced solution (which contains $[\text{Fe}_6\text{C}(\text{CO})_{16}]^{2\ominus}$ and m^-) carried out at 0.3 V led to the formation of $[\text{Fe}_5\text{C}(\text{CO})_{15}]$ and $[\text{M}(\text{CO})_3\text{Cp}]_2$ as detected by IR spectroscopy.

In the case of compound **2**, passivation phenomena precluded exhaustive electrolyses on Pt electrode. However, total reduction was carried out on an Au electrode, which indicated that two electrons were transferred; moreover, a metallic mercury layer on the Au surface was observed at the end of the experiment.

These data indicate that fast Hg-M bond cleavage occurs during the electrochemical reduction of complexes **2-4**, and we propose the mechanism shown in Scheme 1. This mechanism agrees well with those reported for other Hg cluster compounds: m_2Hg ,³² $(\text{PPh}_4)[\text{Fe}_3\{\text{Hg}(\text{m})\}(\text{CO})_{11}]$,⁷ $(\text{PPh}_4)[\text{Mn}_3\{\text{Hg}(\text{m})\}(\text{CO})_{12}(\text{H})]$,³³ and $[\text{Ru}_3\{\text{Hg}(\text{m})\}(\text{CO})_9(\mu_3\text{-}\eta^2\text{-C}=\text{C}^t\text{Bu})]$.³⁴

For all the compounds studied the oxidation step appeared irreversible at 0.1 V s^{-1} and also at higher scan rates (2000 V s^{-1}). Under stationary conditions the study of the limiting current versus the root of electrode rotation speed showed a deviation from linearity for diffusion-controlled process. By comparison with

(30) Rimmelin, J.; Lemoine, P.; Gross, M.; Mathieu, R.; de Montauzon, D. *J. Organomet. Chem.* **1986**, *309*, 355.

(31) (a) Tilset, M. *Inorg. Chem.* **1994**, *33*, 3121. (b) Lacombe, D. A.; Anderson, J. E.; Kadish, K. M. *Inorg. Chem.* **1986**, *25*, 2246. (c) Lacombe, D. A.; Anderson, J. E.; Kadish, K. M. *Inorg. Chem.* **1986**, *25*, 2074. (d) Pampaloni, G.; Koelle, U. *J. Organomet. Chem.* **1994**, *481*, 1.

(32) Lemoine, P.; Giraudeau, A.; Gross, M.; Braunstein, P. *J. Chem. Soc., Chem. Commun.* **1980**, 77.

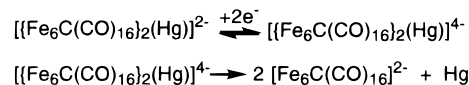
(33) Rossell, O.; Seco, M.; Segalés, G.; Mathieu, R.; de Montauzon, D. *J. Organomet. Chem.* **1996**, *509*, 241.

(34) Osella, D.; Milone, L.; Kukhareenko, S. V.; Strelets, V. V.; Rosenberg, E.; Hajela, S. *J. Organomet. Chem.* **1993**, *451*, 153.

Table 3. Cyclic Voltammetry Data for Compounds **2-5** in Dichloromethane-0.1 M $[\text{n-Bu}_4\text{N}][\text{PF}_6]$ at 0.1 V s^{-1}

	E_p , redn (V)	n	E_p , oxdn (V)	n
2	-0.77	2	0.87	2
3	-0.78	2	0.89	2
4	-0.83	2	0.87	2
5	-0.89	2	0.43	1
			0.79	2

Scheme 2



the height of the reduction wave it can be deduced that two electrons were exchanged but passivation took place either on Pt, Au, or vitreous carbon electrodes precluding further studies.

The cyclic voltammogram of cluster **5** is quite similar to those of **2-4**, with two differences: (i) There is an additional first oxidation wave (0.43 V, $n = 1$), and (ii) a potential shift in the cathodic direction is observed for the reduction (II) and the oxidation (I) waves (Table 3). The coulometry of complexes **5** at -1.2 V requires 2 Faradays/mol, and only $[\text{Fe}_6\text{C}(\text{CO})_{16}]^{2\ominus}$ was formed, which was detected by cyclic voltammetry and IR spectroscopy. This results can be rationalized by Scheme 2.

Although measured potentials are not pure thermodynamic values, we can discuss the uptake (or addition) of the electron. The additional wave at more cathodic potential as well as the shift in the cathodic direction of the reduction wave of **5** compared to **2-4** may arise from the different environment around the Hg atom or, more probably, from the different charge over these clusters. The latter is reinforced by the finding that the complexes $[\{\text{Ru}_3(\text{CO})_9(\mu_3\text{-}\eta^2\text{-C}=\text{C}^t\text{Bu})\}_2(\mu_4\text{-Hg})]$ and $[\text{Ru}_3\{\text{HgMo}(\text{CO})_3\text{Cp}\}(\text{CO})_9(\mu_3\text{-}\eta^2\text{-C}=\text{C}^t\text{Bu})]$, both neutral, show similar electrochemical reduction values³⁴ whereas the oxidation and reduction potentials of the similar but dianionic compound $(\text{PPh}_4)_2[\{\text{Mn}_3(\text{CO})_{12}(\text{H})\}_2(\mu_4\text{-Hg})]$ are shifted to less anodic potential values compared to the monoanionic compounds $(\text{PPh}_4)[\text{Mn}_3\{\text{Hg}(\text{m})\}(\text{CO})_{12}(\text{H})]$.³³

Molecular Orbital Study. Fe_4C Butterfly Compounds. The new cluster $[\text{Fe}_4\text{C}\{\text{AuPPh}_3\}(\text{CO})_{11}(\text{NO})]$ (**7**) has an Fe_4C core nearly identical to that found in all the $[\text{Fe}_4\text{C}\{\text{X}\}_n(\text{CO})_{12}]^{(2-n)-}$ clusters, where $\text{X} = \text{H}$,^{35,36} CO ,³⁷ BH_2 ,³⁸ or AuPR_3 .^{11a,22,39} (Table 4), the X fragments being at either position X_1 or X_2 .

(35) Holt, E. M.; Whitmire, K. H.; Shriver, D. F. *J. Organomet. Chem.* **1981**, *213*, 125.

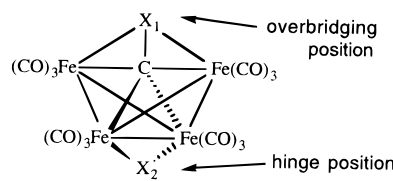
(36) (a) Beno, M. A.; Williams, J. M.; Tachikawa, M.; Muetterties, E. L. *J. Am. Chem. Soc.* **1980**, *102*, 4542. (b) Tachikawa, M.; Muetterties, E. L. *J. Am. Chem. Soc.* **1980**, *102*, 4541. (c) Fehlner, T. P.; Housecroft, C. E. *Organometallics* **1984**, *3*, 764. (d) Housecroft, C. E.; Fehlner, T. P. *Organometallics* **1983**, *2*, 690. (e) Housecroft, C. E. *J. Organomet. Chem.* **1984**, *276*, 297. (f) Housecroft, C. E.; Fehlner, T. P. *Organometallics* **1986**, *5*, 1279. (g) Phosphine-substituted compound: Wade, H.; Braga, D.; Grepioni, F. *Organometallics* **1995**, *14*, 24.

(37) Bradley, J. S.; Ansell, G. B.; Leonowicz, M. E.; Hill, E. W. *J. Am. Chem. Soc.* **1981**, *103*, 4968.

(38) (a) Meng, X.; Rath, N. P.; Fehlner, T. P. *J. Am. Chem. Soc.* **1989**, *111*, 3422. (b) *Organometallics* **1991**, *10*, 1986.

(39) Bogdan, P. L.; Horwitz, C. P.; Shriver, D. F. *J. Chem. Soc., Chem. Commun.* **1986**, 553.

(40) Davis, J. H.; Beno, M. A.; Williams, J. M.; Zimmie, J.; Tachikawa, M.; Muetterties, E. L. *Proc. Natl. Acad. Sci. U.S.A.* **1981**, *78*, 668.

Table 4. Compounds with the Same Butterfly Fe₄C Core


compd	X ₁	α	X ₂	β	ref
A		153		147	40
B		155	H	158	35
C			CO		37
D	H ^a	164	H	160	36
E	BH ₂	163	H	158	38
F	AuPR ₃		H		11a
G	AuPR ₃				39
G	AuPR ₃	158		146	this work (7)
H ^b	AuPR ₃	167	CO	166	22
J			AuPR ₃		hypothetical

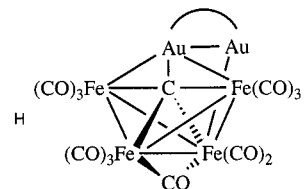
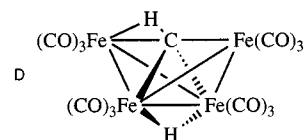
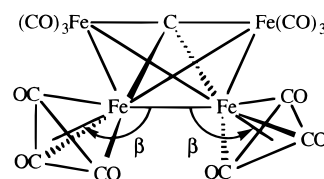
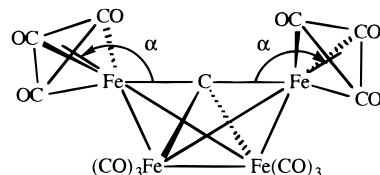
^a The H atom is not located exactly at X₁ but tilted in order to bridge one of the Fe_w–C bonds (Chart 2). ^b In this case the gold fragment is Au₂(μ-dppm), with one gold atom placed at X₁ and the other one bonded to a hinge iron (see Chart 2).

While H⁺ preferred to bridge the hinge (position X₂), the AuPR₃⁺ units were always found overbridging the butterfly (position X₁). Although the structure of the compound [Fe₄C{AuPPh₃}₃(CO)₁₂][−] (G) was not determined by X-ray diffraction, the wingtip-bridged butterfly structure proposed³⁹ is confirmed by comparing its spectroscopic data with those of the compound [Fe₄C{AuPPh₃}₃(CO)₁₁(NO)] (7). In particular, the ¹³C NMR of both compounds showed very similar values of ²J_{C–p}.

Some of these clusters had been extensively studied due to their interest as models for surface chemistry and for the reactivity of the carbide carbon. Theoretical studies have been carried out for the clusters A–D.^{41,42} Bradley et al. showed the [Fe₄C(CO)₁₂]^{2−} HOMO to be basically located at the hinge, thus explaining the bonding of the additional group at the hinge in [HFe₄C(CO)₁₂][−], [(μ-CO)Fe₄C(CO)₁₂], and [HFe₄C{H}(CO)₁₂]. However, such an orbital cannot explain the structure of the Au derivatives (G), in which the hinge position is vacant. When a second X fragment was added to [HFe₄C(CO)₁₂][−] (D–F), it bonded at the C atom (position X₁), and for BH₂⁺ and AuPR₃⁺ it had been claimed that a π interaction with the p-orbital takes place. In fact, for [HFe₄{BH₂}₂(CO)₁₂] Fenske–Hall calculations^{38b} showed significant π interaction between the boron atom and the HFe₄C(CO)₁₂ fragment.

Since carbonyl reorganization and metal framework motions are relatively low-energy processes,⁴³ we compared all these structures looking for structural differences, and found that the Fe₄C core is nearly identical for all of them except for the CO orientations that change upon coordinating an X fragment.

The different arrangement of the CO ligands in the compounds studied can be represented by the angle α for the wingtip carbonyls and by β for the hinge carbonyls (see Chart 3). In the bare cluster [Fe₄C(CO)₁₂]^{2−}, both angles are close to 150°. Whenever there was a group bridging the hinge, the β angle was larger:

Chart 2**Chart 3**

158–160° for hydrido bridges (compounds B, D, and E) or 166° for a CO bridge (H, Chart 2, Chart 3). Similarly, the presence of a group overbridging the butterfly opened up the α angle: 158–167° in compounds D, E, G, and H (see Table 4).

We have carried out extended Hückel calculations on a model cluster [Fe₄C(CO)₁₂]^{2−} in order to study (a) the effects of the CO orientation on the frontier orbitals and the preferred bonding position and (b) the importance of π-bonding for site preference.

The MO scheme for a model fragment [Fe₄C(CO)₁₂]^{2−} (A) using the mean distances Fe–C and Fe–Fe of the different compounds (A–H) was calculated for α and β values ranging from 130 to 178° (Figure 4). The most stable structure for the bare cluster is found for α = 162° and β = 145°. These values are in fair agreement with the experimental values of A (153 and 147°, respectively).

The highest occupied orbitals obtained for fragment A are similar to those found by Bradley.⁴¹ Two important types of orbital can be distinguished, those mostly directed toward the overbridging position (1a₁ and 2b₂, Figure 5) and those pointing toward the hinge position (2a₁ and 1b₁, Figure 6). Thus the interactions of A with an X fragment in one or other position can be approximately considered as independent. 2a₁ and 1a₁ can originate sigma bonds whereas 2b₂ and 1b₁ form π bonds with an X fragment. Both 1a₁ and 1b₁ orbitals have a significant carbide contribution (around 20% p_z and 15% p_x, respectively).

At the orbital level, the main effect of increasing β is a rehybridization of the 2a₁ and 1b₁ orbitals, which become better oriented to interact with an incoming X group at the hinge (Figure 6). In a similar way, when α increases, 2b₂ and 1a₁ are better directed to position

(41) Harris, S.; Bradley, J. S. *Organometallics* **1984**, *3*, 1086.

(42) Wijeyesekera, S. D.; Hoffmann, R.; Wilker, C. N. *Organometallics* **1984**, *3*, 962.

(43) Whitmire, K. H. *J. Coord. Chem.* **1988**, *17*, 95.

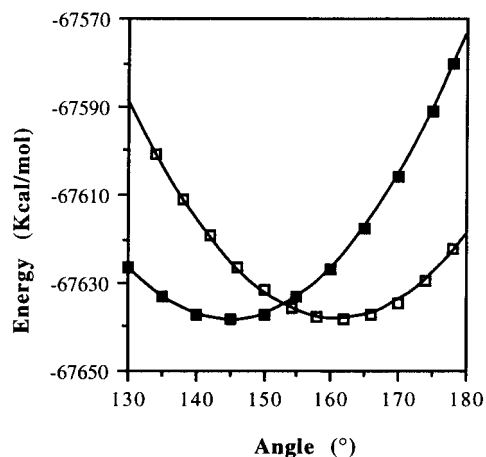


Figure 4. Plot of the total energy calculated for the model $[\text{Fe}_4\text{C}(\text{CO})_{12}]^{2-}$ versus the variation of angle β (■) from 130 to 178° with $\alpha = 162^\circ$ and of angle α (□) from 130 to 178° with $\beta = 145^\circ$.

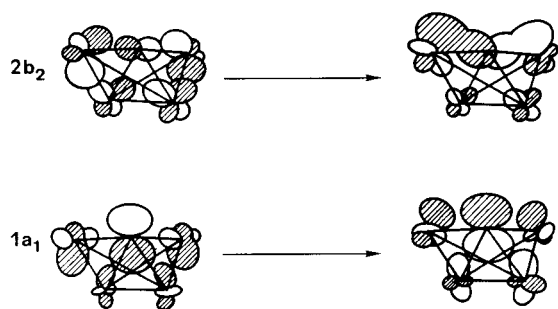


Figure 5. Rehybridization of $2b_2$ and $1a_1$ on increasing α from 150 to 178° with $\beta = 145^\circ$.

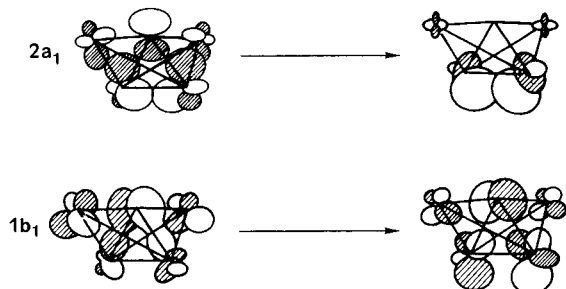


Figure 6. Rehybridization of $2a_1$ and $1b_1$ on increasing β from 145 to 178° with $\alpha = 162^\circ$.

X_1 (see Figure 5). The effect of these reorientations on the total energy can be seen with two examples: (i) Increasing the β value of $[\text{HFe}_4\text{C}(\text{CO})_{12}]^-$ (B) from 145 to 160° produces a 12.0 kcal/mol stabilization. (ii) When the α angle of $[\text{Fe}_4\text{C}\{\text{AuPH}_3\}(\text{CO})_{12}]^-$ (G) is increased from 150 to 158°, the compound is stabilized by 8.3 kcal/mol.

Site Preference. (a) The AuPH_3^+ Fragment. The phenyl groups of the gold fragment were substituted by hydrogen groups for simplicity; thus, calculations were carried out for $X = \text{AuPH}_3^+$ in both positions (1 and 2). The difference in energy between them is small, the compound with the gold fragment bridging the wings (model G) being 4 kcal/mol more stable than at the hinge position (model J), if the β value for this latter compound is assumed to be at least 160°.

When the AuPH_3^+ fragment overbridges the $[\text{Fe}_4\text{C}(\text{CO})_{12}]^{2-}$ butterfly, the bonding between the two fragments occurs mostly through the $1a_1$ and $2b_2$

orbitals, as expected. The overlap populations between atoms obtained in this case (model G, Table 5) clearly show that there is strong Au–C bonding and weak gold–wingtip iron bonding and that only the carbide–wingtip iron bonds are weakened, although these bonds remain stronger than the carbide–hinge iron ones. All this suggests that the interaction between AuPH_3^+ and A is basically a σ bond centered at the C atom reinforced by a π interaction, as has been seen for $[\text{HFe}_4\text{C}\{\text{BH}_2\}(\text{CO})_{12}]$.^{38b}

An increase of the angle α enhances the overlap population of the Au–C and C– Fe_w bonds. The most stable structure was obtained for $\alpha = 162^\circ$ and $\beta = 146^\circ$, in good agreement with that found for compound 7 ($\alpha = 158^\circ$, $\beta = 146^\circ$).

When the AuPH_3^+ fragment is added at the hinge (model J), this fragment bonds mainly through its LUMO with the $2a_1$ orbital of $[\text{Fe}_4\text{C}(\text{CO})_{12}]^{2-}$. A π -interaction involving $1b_1$ also takes place, but the overlap population shows that this interaction is weaker than that obtained when the gold fragment is over the wingtip edge.

The energy for this model J depends on the angle chosen, the most stable geometry appearing at $\beta = 152^\circ$. In this case the total energy is very similar to (0.74 kcal/mol greater than) that found for model G. The fact that gold fragments are found overbridging the butterfly but not at the hinge of the cluster is probably associated with the steric demand of the phosphine ligand. Indeed, in $[\text{Fe}_4\{\text{AuPet}_3\}(\mu_4\text{-CO})(\text{CO})_{12}]^-$, which also has a related butterfly geometry¹⁴ (Chart 4), in which the AuPet_3 unit bridges the hinge, the angle between the hinge carbonyl groups is $\beta = 163^\circ$. Increasing β in model J from the optimum value of 152 to 160° requires 3.5 kcal/mol, making this structure 4.2 kcal/mol less stable than the wingtip-bridged one (model G). This steric problem is of course aggravated for the bulkier PPh_3 ligands in compounds G.

(b) The H^+ Fragment. For $X = \text{H}^+$ bridging the wingtip edge, the interaction with the H-1s orbital occurs mainly through the $1a_1$ and, for H^+ bridging the hinge edge, through the $2a_1$ orbital. If H^+ in the first position is tilted to adopt the experimental geometry (D), a 0.24 eV stabilization results due to the contribution of the $2b_2$ orbital to the bonding. This interaction is possible because of the absence of a H–C π bond.

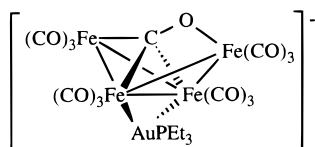
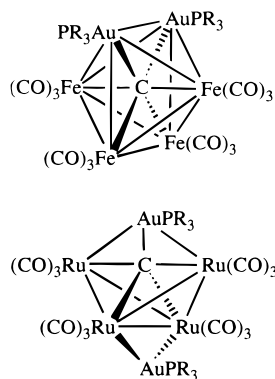
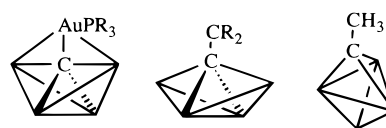
Let us now compare the compounds with $X = \text{H}^+$ at the carbide atom (tilted as in D, Chart 2) and at the hinge (compound B). As $2a_1$ has a better topology to interact with the 1s orbital than $1a_1$ (the $2a_1/1s$ overlap population, 0.55, was much greater than the $1a_1/1s$ one, 0.22), the hinge-bridged structure is 1.3 eV more stable, in good agreement with the experimental structure of $[\text{HFe}_4\text{C}(\text{CO})_{12}]^-$. The atomic charge on the H atom was 0.139 when the H bridges a carbide–iron edge and -0.174 when this atom bridges the hinge. Thus, in these structures the differences in energy and in atomic charge suggest that the different position of the AuPR_3^+ and H^+ fragments could arise from the ability of the H atom to adopt an hydridic character.

(c) The CO Fragment. When $X = \text{CO}$ was added at the hinge (compounds C and H), there was a strong σ -bond through the $2a_1$ orbital and an important π -interaction through the $1b_1$ orbital. If the CO ligand is added at the carbide site, a much stronger π -interaction

Table 5. Overlap Population Calculated for Different Atom Pairs in the Two Models of the Anion $[\text{Fe}_4\text{C}\{\text{AuPPh}_3\}(\text{CO})_{12}]^-$ ^a

X = AuPH ₃	Au–C	Au–Fe _w	Au–Fe _h	C–Fe _w	C–Fe _h	Fe _h –Fe _h
model G (X ₁): α = 160, β = 146	0.370	0.071	–0.016	0.629 (0.723)	0.437 (0.438)	0.239 (0.240)
model J (X ₂): α = 160, β = 155	–0.001	–0.002	0.157	0.726 (0.725)	0.427 (0.429)	0.186 (0.262)

^a The numbers in parentheses are the overlap population values of the bare cluster with the same α and β angles.

Chart 4**Chart 5****Chart 6**

occurs with the orbitals of the cluster 2b₂ and 1b₂ (lying at lower energy, with a sizable contribution from C-p_y). However, in this case, the σ-interaction through 1a₁ is much weaker and the structure is some 60 kcal/mol less stable.

Compounds with Two Gold Fragments. If a second gold unit is added, the MO scheme obtained for $[\text{Fe}_4\text{C}(\text{CO})_{12}]^{2-}$ can also be used to explain the compound structure. In the case of $[\text{Fe}_4\text{CAu}_2(\text{CO})_{12}(\mu\text{-dppm})]$ (H in Chart 2),²² one Au atom bonds to a hinge iron producing a rotation of the carbonyl ligands around this atom, one of the CO becoming semibridging along the Fe–Fe hinge. The same reorganization was observed in a related compound, $[\text{HFe}_4\text{B}\{\text{AuPPh}_3\}_2(\text{CO})_{12}]$.⁴⁴ This carbonyl ligand is allowed to interact with 2a₁ and 1b₁ (hinge position) while the Au(1) atom interacts with 1a₁ and 2b₂. The α and β angles calculated for a $[(\mu\text{-CO})\text{Fe}_4\text{C}\{\text{AuPH}_3\}(\text{CO})_{12}]^+$ model were 166 and 165°, in excellent agreement with the experimental value for $[\text{Fe}_4\text{CAu}_2(\text{CO})_{12}(\mu\text{-dppm})]$ of 167 and 166°, respectively.

Considering this MO scheme, one would expect $[\text{Fe}_4\text{C}\{\text{AuPEt}_3\}_2(\text{CO})_{12}]^{11a}$ to adopt the structure of $[\text{Ru}_4\text{C}\{\text{AuPR}_3\}_2(\text{CO})_{12}]^{45}$ with one gold fragment over the wingtip Fe–C–Fe edge and the other bridging the hinge, instead of the actual octahedral structure (see Chart 5). Unfortunately the α and β values for this compound are not available. Our calculations on an idealized octahedral model show the most stable form to have α = 166° and β = 143° but no significant overlap population appears between the Au and hinge iron atoms, and the bonding energy between the $\text{Au}_2(\text{PH}_3)_2^{2+}$ and $[\text{Fe}_4\text{C}(\text{CO})_{12}]^{2-}$ fragments is almost negligible (2.1

kcal/mol). Perhaps here the stabilization of the X⁺ fragment at the hinge is surpassed by the d¹⁰–d¹⁰ interaction. However, it is difficult to explain why this compound does not adopt the structure of $[\text{Fe}_4\text{CAu}_2(\text{CO})_{12}(\mu\text{-dppm})]$ (compound H)²². The fluxional behavior of the latter compound at room temperature (the two phosphorus atoms become equivalent) is easily explained in terms of an octahedral structure. Thus, this seems to be energetically accessible even for compound H, suggesting that a small energetic gain in crystal packing could be enough for $[\text{Fe}_4\text{C}\{\text{AuPEt}_3\}_2(\text{CO})_{12}]$ to prefer this structure in the solid state.

Related Compounds. Finally, it is interesting to compare $[\text{Fe}_4\text{C}\{\text{X}\}_n(\text{CO})_{12}]^{(2-n)-}$ with the related $[\text{Fe}_4\text{C}\{\text{CR}_2\}(\text{CO})_{12}]^-$ and $[\text{Fe}_4\text{C}\{\text{CH}_3\}(\text{CO})_{12}]^-$ compounds.⁴⁶ The structure of the Fe₄C skeleton in the $[\text{Fe}_4\text{C}\{\text{CR}_2\}(\text{CO})_{12}]^-$ clusters presents two important differences (see Chart 6): The Fe_w–C–Fe_w mean angle is now 150° (cf. 175°), and the mean of the dihedral angle between the wings is 127° (cf. 106°). The difference is due to the stronger π bond between the C and CR₂ atoms, which weakens the C–Fe_w bond much more than the AuPR₃⁺ or BH₂⁺ units. Thus, the number of electrons in the $[\text{Fe}_4\text{C}(\text{CO})_{12}]$ fragment cluster decreases and the structure opens. When CR₂ is replaced by a CH₃ fragment, the $[\text{Fe}_4\text{C}\{\text{CH}_3\}(\text{CO})_{12}]^-$ butterfly structure cannot be stabilized by a C–CH₃ π-interaction, and it becomes tetrahedral.

Experimental Section

All manipulations were performed under an atmosphere of prepurified N₂ with standard Schlenk techniques, and all solvents were distilled from appropriate drying agents. Elemental analyses of C, H, and N were carried out at the Institut de Bio–Orgànica de Barcelona. Infrared spectra were recorded in THF solutions on an FT-IR 520 Nicolet spectrophotometer. ³¹P{¹H} NMR spectra were obtained on a Varian XL-200 spectrometer (δ(TMS) = 0.0 ppm). ¹³C{¹H} NMR spectra were obtained on a Varian Unity 300 MHz spectrometer. FABMS and electrospray mass spectra were recorded in a Fisons VG Quattro spectrometer with methanol as solvent. The compounds ClAuPPh₃,⁴⁷ ClHg(m)⁴⁸ (m = Mo(CO)₃Cp, W(CO)₃Cp, and Mn(CO)₅), and (NEt₄)₂[Fe₆C(CO)₁₆]¹⁹ were synthesized as described previously.

Synthesis of $[\text{NEt}_4][\text{Fe}_6\text{C}\{\text{AuPPh}_3\}(\text{CO})_{16}]$ (1). Solid ClAuPPh₃ (0.56 g, 1.13 mmol) and TIBF₄ (0.33 g, 1.13 mmol)

(44) Housecroft, C. E.; Rheingold, A. L. *Organometallics* **1987**, *6*, 1332.

(45) Cowie, A. G.; Johnson, B. F. G.; Lewis, J.; Raithby, P. R. *J. Chem. Soc., Chem. Commun.* **1984**, 1710.

(46) (a) Bogdan, P. L.; Woodcock, C.; Shriver, D. F. *Organometallics* **1986**, *6*, 1377 and references therein. (b) Bradley, J. S.; Harris, S.; Newsam, J. M.; Hill, E. W.; Leta, S.; Modrick, M. A. *Organometallics* **1987**, *6*, 2060. (c) Wang, J.; Crespi, A. M.; Sabat, M.; Harris, S.; Woodcock, C.; Shriver, D. F. *Inorg. Chem.* **1989**, *28*, 697. (d) Bradley, J. S.; Harris, S.; Hill, E. W.; Modrick, M. A. *Polyhedron* **1990**, *9*, 1809.

(47) Kowala, C.; Swan, J. M. *Aust. J. Chem.* **1966**, *19*, 547.

(48) Mays, M. J.; Robb, J. D. *J. Chem. Soc. A* **1968**, 329.

were added to a solution of $(\text{Et}_4\text{N})_2[\text{Fe}_6\text{C}(\text{CO})_{16}]$ (1.20 g, 1.14 mmol) in THF (40 mL) at -15°C . In 30 min the color changed from dark violet to black. The solution was stirred for 7 h, filtered through Celite, and concentrated to half the volume. Then, diethyl ether (20 mL) was slowly added. Black crystals of $(\text{Et}_4\text{N})[\text{Fe}_6\text{C}\{\text{AuPPh}_3\}(\text{CO})_{16}]$ were obtained after cooling overnight (yield 1.21 g, 77%). IR (THF, cm^{-1}): $\nu(\text{CO})$ stretch 2042 m, 1987 vs, 1965 s (sh), 1801 w. $^{31}\text{P}\{^1\text{H}\}$ NMR (240 K, THF, $\delta(\text{ppm})$): 55.6. $^{13}\text{C}\{^1\text{H}\}$ NMR (295 K, CD_2Cl_2 , $\delta(\text{ppm})$): 224.6 (CO), 228.6 (CO), 499.9 (C). ESMS (M^-) (m/z): calc, 1255; found, 1255. Anal. Calc: C, 37.28; H, 2.53; N, 1.01. Found: C, 37.19; H, 2.61; N, 1.02.

Synthesis of $[\text{NEt}_4][\text{Fe}_6\text{C}\{\text{Hg}(\text{m})\}(\text{CO})_{16}]$ ($\text{m} = \text{Mo}(\text{CO})_3\text{Cp}$ (2**), $\text{W}(\text{CO})_3\text{Cp}$ (**3**), $\text{Mn}(\text{CO})_5$ (**4**)).** Details of synthesis of **2** also apply to **3** and **4**. Solid $\text{ClHgMo}(\text{CO})_3\text{Cp}$ (0.16 g, 0.33 mmol) was added to a solution of $(\text{Et}_4\text{N})_2[\text{Fe}_6\text{C}(\text{CO})_{16}]$ (0.18 g, 0.17 mmol) in THF (20 mL) at 0°C . The solution was stirred for 20 h at this temperature and then filtered through Celite and evaporated to dryness. The residual solid was washed twice with toluene (2×10 mL) and dried in vacuo. Recrystallization in acetone/methanol gave dark crystals of $(\text{Et}_4\text{N})[\text{Fe}_6\text{C}\{\text{HgMo}(\text{CO})_3\text{Cp}\}(\text{CO})_{16}]$ (**2**) (yield 0.15 g, 65%). IR (THF, cm^{-1}): $\nu(\text{CO})$ stretch 2052 w, 1999 vs, 1988 vs, 1919 m, 1886 w, 1825 w. $^{13}\text{C}\{^1\text{H}\}$ NMR (295 K, CD_2Cl_2 , $\delta(\text{ppm})$): 222.4 (br, CO), 216.6 (CO). ESMS (m/z): (M^-) 1241, ($M - 4\text{CO}$) 1129. Anal. Calc: C, 28.89; H, 1.82; N, 1.02. Found: C, 28.98; H, 1.87; N, 1.05. Yield for **3**: 0.18 g, 60%. IR (THF, cm^{-1}): $\nu(\text{CO})$ stretch 2052 m, 1999 s, 1987 vs, 1896 w, 1880 m, 1822 w. $^{13}\text{C}\{^1\text{H}\}$ NMR (295 K, CD_2Cl_2 , $\delta(\text{ppm})$): 222.3 (br, CO), 216.5 (CO). ESMS (m/z): ($M - 4\text{CO}$) 1217. Anal. Calc: C, 27.15; H, 1.71; N, 0.96. Found: C, 27.29; H, 1.79; N, 1.01. Yield for **4**: 0.12 g, 55%. IR (THF, cm^{-1}): $\nu(\text{CO})$ stretch 2081 w, 2046 m, 2009 (sh), 1992 vs, 1825 w. $^{13}\text{C}\{^1\text{H}\}$ NMR (295 K, CD_2Cl_2 , $\delta(\text{ppm})$): 223.7 (CO), 206.9 (CO). ESMS (m/z): ($M - 4\text{CO}$) 1079. Anal. Calc: C, 27.26; H, 1.51; N, 1.06. Found: C, 27.39; H, 1.60; N, 1.10.

Synthesis of $[\text{NEt}_4]_2[\{\text{Fe}_6\text{C}(\text{CO})_{16}\}_2(\text{Hg})]$ (5**).** Solid $\text{Hg}(\text{NO}_3)_2$ (34 mg, 0.10 mmol) was added to a solution of $(\text{Et}_4\text{N})_2[\text{Fe}_6\text{C}(\text{CO})_{16}]$ (0.12 g, 0.11 mmol) in THF (20 mL) at room temperature. The solution was stirred for 20 h and then filtered through Celite and evaporated to dryness. The residual solid was extracted with 5 mL of methanol. The solution obtained was concentrated to half-volume and cooled overnight. Dark brown crystals of $(\text{Et}_4\text{N})_2[\{\text{Fe}_6\text{C}(\text{CO})_{16}\}_2(\text{Hg})]$ were obtained (yield 31 mg, 30%). IR (THF, cm^{-1}): $\nu(\text{CO})$ stretch 2038 m, 2010 vs, 1988 (sh), 1965 w, 1819 w. ESMS (m/z): [$M(\text{Et}_4\text{N}) - 8\text{CO}$] 1698; [$M - 8\text{CO}$] 784. Anal. Calc: C, 29.26; H, 1.95; N, 1.36. Found: C, 29.45; H, 2.09; N, 1.38.

Synthesis of $[\text{Fe}_6\text{C}\{\text{AuPPh}_3\}(\text{CO})_{15}(\text{NO})]$ (6**).** Solid NOBF_4 (53 mg, 0.45 mmol) was added to a solution of $(\text{Et}_4\text{N})[\text{Fe}_6\text{C}\{\text{AuPPh}_3\}(\text{CO})_{16}]$ (0.57 g, 0.41 mmol) in THF (35 mL) at 5°C . The resulting solution was stirred at this temperature for 5 h, then more NOBF_4 (48 mg, 0.41 mmol) was added and the solution stirred for a further 1.5 h. After filtering of the solution through Celite, the solvent was evaporated in vacuo. The product was extracted with toluene (2×20 mL), and the solution was filtered and evaporated to dryness. All attempts to crystallize this compound were unsuccessful; in all cases a mixture of it and $[\text{Fe}_4\text{C}\{\text{AuPPh}_3\}(\text{CO})_{11}(\text{NO})]$ (**7**) was obtained along with other decomposition products. IR (THF, cm^{-1}): $\nu(\text{CO})$ stretch 2058 m, 2005 vs, 1989 m, 1839 w, 1812 sh, 1754 w. $^{31}\text{P}\{^1\text{H}\}$ NMR (240 K, THF, $\delta(\text{ppm})$): 54.0.

Synthesis of $[\text{Fe}_4\text{C}\{\text{AuPPh}_3\}(\text{CO})_{11}(\text{NO})]$ (7**).** Solid NOBF_4 (89 mg, 0.76 mmol) was added to a solution of $(\text{Et}_4\text{N})[\text{Fe}_6\text{C}\{\text{AuPPh}_3\}(\text{CO})_{16}]$ (0.53 g, 0.38 mmol) in THF (35 mL) at 5°C . The resulting solution was stirred at this temperature for 30 min, then more NOBF_4 (89 mg, 0.76 mmol) was added, and the solution was stirred for 4 h at 5°C . After the solution was filtered through Celite, the solvent was evaporated in vacuo. The product was extracted with toluene (2×15 mL), and the resulting solution was filtered and evaporated to dryness. The residue was dissolved in 10 mL of THF. After

the solution was layered with MeOH (10 mL) and cooled overnight, dark green crystals of $[\text{Fe}_4\text{C}\{\text{AuPPh}_3\}(\text{CO})_{11}(\text{NO})]$ were obtained (yield 0.18 g, 46%). IR (THF, cm^{-1}): $\nu(\text{CO})$ stretch 2070 w, 2030 s, 2005 vs, 1988 s (sh), 1762 m. $^{31}\text{P}\{^1\text{H}\}$ NMR (240 K, THF, $\delta(\text{ppm})$): 38.8. $^{13}\text{C}\{^1\text{H}\}$ NMR (295 K, CD_2Cl_2 , $\delta(\text{ppm})$): 212.2 (CO), 213.9 (CO), 218.4 (CO), 443.4 (d, C, $^2J_{\text{C-P}} = 53$ Hz). FABMS (NBA matrix): ($M - 2\text{CO}$) 977. Anal. Calc: C, 34.87; H, 1.45; N, 1.36. Found: C, 35.04; H, 1.51; N, 1.36.

Electrochemical Measurements. Electrochemical measurements were carried out with an Electrostat⁴⁹ using the interrupt method to minimize the uncompensated resistance (IR) drop. Electrochemical experiments were performed at room temperature in an airtight three-electrode cell connected to a vacuum argon/ N_2 line. The reference electrode consisted of a saturated calomel electrode (SCE) separated from the nonaqueous solutions by a bridge compartment. The counter electrode was a spiral of ca. 1 cm^2 apparent surface area, made of Pt wire 8 cm long and 0.5 mm in diameter. The working electrode was Pt (1 mm i.d.), Au (2 mm i.d.), or vitreous carbon (2 mm i.d.) for cyclic voltammetry or a rotating disk electrode of Pt or Au disk with a diameter of 2 mm for linear voltammetry. For electrolysis experiments a Pt or Au gauze or foil was used. The supporting electrolyte was $[\text{n-Bu}_4\text{N}][\text{PF}_6]$ (Fluka electrochemical grade), used as received. All solutions measured were $(0.5-1.0) \times 10^{-3}$ M in the organometallic complex and 0.1 M in supporting electrolyte. Under the same conditions ferrocene was oxidized at $E^\circ = 0.42$ V.

Computational Details. The extended Hückel calculations were carried out using the program CACAO⁵⁰ with the parameters found in the literature for Fe, Au, C, O, H, and P atoms.⁵¹ The model $[\text{Fe}_4\text{C}(\text{CO})_{12}]^{2-}$ was constructed with the mean distances $\text{Fe}_w\text{-C} = 1.85$, $\text{Fe}_h\text{-C} = 1.95$, $\text{Fe}_w\text{-Fe}_h = 2.65$, and $\text{Fe}_h\text{-Fe}_h = 2.58$ Å. For all the CO ligands the Fe-C-O angle was considered to be 180° and the Fe-C and C-O distances were 1.78 and 1.18 Å, respectively. All the OC-Fe-CO angles were idealized to 90° . When an X fragment was added, the X-C or X-Fe_h distances used were those found in the literature^{22,35-38} and in compound **7**. For the hypothetical model J (the AuPH₃ bridging the hinge) the Fe-Au distance found in $[\text{Fe}_4\text{C}\{\text{AuPEt}_3\}(\mu_4\text{-CO})(\text{CO})_{12}]^-$ (2.67 Å)¹⁴ was used (similar to those found for Fe_2Au^2 and Fe_3Au^7 clusters). For the imaginary compound with a CO ligand at the carbide, C-C distances from 1.43 to 1.60 Å were used to cover the distances found in $[\text{Fe}_4\{\text{C}=\text{C}(\text{OCH}_3)_2\}(\text{CO})_{12}]$ (1.44 Å),^{46d} $[\text{Fe}_4\text{C}\{\text{COCH}_3\}(\text{CO})_{12}]$ (1.49 Å),^{46b} and the sum of the covalent radii (1.54 Å).

The α and β angles were calculated with the Cerius2 program (Molecular Simulations Ltd.) using the structural data available from the Cambridge Structural Database.⁵²

X-ray Data Collection, Structure Determination, and Refinement for $(\text{NEt}_4)[\text{Fe}_6\text{C}\{\text{AuPPh}_3\}(\text{CO})_{16}]$ (1**) and $[\text{Fe}_4\text{C}\{\text{AuPPh}_3\}(\text{CO})_{11}(\text{NO})]$ (**7**).** Crystallographic data are summarized in Table 6. A total of 10 749 (**1**) and 7680 (**7**) unique reflections were measured with θ in the range $3-27^\circ$; 3271 having $I > 3\sigma(I)$, for **1**, and 3784 having $I > 2\sigma(I)$, for **7**, were used in the refinement. One standard reflection was monitored every 100 measurements; no significant decay was noticed over the time of data collection. Intensities were corrected for Lorentz and polarization effects. An empirical correction for absorption was applied.⁵³

(49) Cassoux, P.; Dartiguepeyron, R.; David, C.; de Montauzon, D.; Tommasino, J. B.; Fabre, P. L. *Actual. Chim.* **1994**, *1*, 49.

(50) Mealli, C.; Proserpio, D. M. Computer Aided Composition of Atomic Orbitals, C.A.C.A.O. Program, Version 4.0, 1994. *J. Chem. Educ.* **1990**, *67*, 399.

(51) Komiya, S.; Albright, T. A.; Hoffmann, R.; Kochi, J. K. *J. Am. Chem. Soc.* **1977**, *99*, 8440. Hoffmann, R. *J. Chem. Phys.* **1963**, *39*, 1397. Summerville, R. H.; Hoffmann, R. *J. Am. Chem. Soc.* **1976**, *98*, 7240.

(52) Allen, F.; Kennard, O.; Taylor, R. *Acc. Chem. Res.* **1983**, *16*, 146.

Table 6. Crystallographic Data for 1 and 7

mol formula	[C ₈ H ₂₀ N]- [C ₃₅ H ₁₅ AuFe ₆ O ₁₆ P]	[C ₃₀ H ₁₅ AuFe ₄ NO ₁₂ P]
fw	1384.77	1032.78
cryst system	monoclinic	monoclinic
space group	<i>P</i> 2 ₁ / <i>c</i>	<i>P</i> 2 ₁ / <i>n</i>
radiatn (Å)	Mo Kα graphite-monochromated (λ = 0.710 73)	
diffractometer	Siemens AED	Philips PW 1100
<i>a</i> , Å	10.233(2)	17.142(5)
<i>b</i> , Å	22.464(4)	15.738(2)
<i>c</i> , Å	21.530(5)	13.771(4)
β, deg	92.78(2)	108.63(2)
<i>V</i> , Å ³	4943(2)	3520(2)
<i>Z</i>	4	4
<i>D</i> _{calcd} , g cm ⁻³	1.861	1.949
<i>F</i> (000)	2712	1984
μ(Mo Kα), cm ⁻¹	47.67	58.67
max, min transm factors	1.00–0.548	1.00–0.614
GOF ^a	1.09	1.09
<i>R</i> (<i>F</i> _o) ^b	0.0510	0.0360
<i>R</i> (<i>F</i> _o) ^c	0.0574	0.0441

^a GOF = $[\sum w(|F_o| - |F_c|)^2 / (N_{\text{observns}} - N_{\text{var}})]^{1/2}$. ^b $R = \sum |F_o| - |F_c| / \sum |F_o|$. ^c $R_w = [\sum w(|F_o| - |F_c|)^2 / \sum w(F_o)^2]^{1/2}$.

The structures were solved by direct and Fourier methods and refined first by full-matrix least-squares procedures with isotropic thermal parameters and then in the last cycles of refinement by blocked-matrix least-squares procedures with anisotropic thermal parameters for the non-hydrogen atoms, excepting the carbons of the phenyl rings for **1**, and by full-matrix least squares procedures with anisotropic thermal parameters for the non-hydrogen atoms for **7**. In the isotropic refinement of **7** 12 carbonyl groups were considered, because of the difficulty to distinguish with certainty a nitrosyl versus a carbonyl ligand. Moreover a disordered distribution of the nitrosyl group over all positions of the carbonyls was taken into account. However at the end of the isotropic refinement some evidence was found about the location of the nitrosyl ligand: (i) Only the isotropic thermal parameters of the C and O atoms of a carbonyl, C(11) and O(11), resulted in being very different, whereas they were comparable for all remaining carbonyls. The thermal parameters at the end of the isotropic refinement after replacing the C(11) atom with the nitrogen atom N(11) resulted in being comparable. (ii) The Fe(4)–N(11)

(53) Walker, N.; Stuart, D. *Acta Crystallogr.* **1983**, *A39*, 158. Gozzoli, F. *Comput. Chem.* **1987**, *11*, 109.

bond distance was found in every stage of the refinement to be shorter than the Fe–C ones involving carbonyls. Finally the same evidence was found from a second data set obtained from a different crystal. In this way the position of the nitrosyl group was reasonably assigned. All hydrogen atoms were placed at their geometrically calculated positions (C–H = 0.96 Å) and refined “riding” on the corresponding carbon atoms, isotropically. The final cycles of refinement were carried out on the basis of 525 (**1**) and 443 (**7**) variables; after the last cycles, no parameters shifted by more than 0.15 (**1**) and 0.12 (**7**) times their esd. The highest remaining peak in the final difference map (close to the gold atom) was equivalent to about 0.84 (**1**) and 1.21 (**7**) e/Å³. In the final cycles of refinement a weighting scheme $w = K[\sigma^2(F_o) + gF_o^2]^{-1}$ was used; at convergence the *K* and *g* values were 1.210 and 0.0009 for **1** and 0.611 and 0.0013 for **7**. Final *R* and *R_w* values were 0.0510 and 0.0574 for **1** and 0.0360 and 0.0441 for **7**. The analytical scattering factors, corrected for the real and imaginary parts of anomalous dispersion, were taken from ref 54. All calculations were carried out on the Gould Povernode 6040 and Encore 91 computers of the “Centro di Studio per la Strutturistica Diffrattometrica” del CNR, Parma, Italy, using the SHELX-76 and SHELXS-86 systems of crystallographic computer programs.⁵⁵

Acknowledgment. Financial support for this work was generously given by the DGICYT (Spain) through Grants PB93-0766 and PB92-0655. G.S. is indebted to the Ministerio de Educación y Ciencia for a scholarship. We thank R. Mathieu for fruitful discussions.

Supporting Information Available: Tables of final values of atomic coordinates for the non-hydrogen atoms, calculated coordinates and isotropic thermal parameters for the hydrogen atoms, anisotropic thermal parameters for some of the non-hydrogen atoms, and complete bond distances and angles for compounds **1** and **7** (19 pages). Ordering information is given on any current masthead page.

OM9605802

(54) *International Tables for X-ray Crystallography*; Kynoch Press: Birmingham, England, 1974; Vol. IV.

(55) Sheldrick, G. M. SHELX-76 Program for crystal structure determination, University of Cambridge, England, 1976; SHELXS-86 Program for the solution of crystal structures, University of Göttingen, 1986.